MSGNav: Unleashing the Power of Multi-modal 3D Scene Graph for Zero-Shot Embodied Navigation

Xun Huang^{1,2} Shijia Zhao¹ Yunxiang Wang³ Xin Lu^{2,4}
Wanfa Zhang¹ Rongsheng Qu^{2,5} Weixin Li^{2,5} ✓ Yunhong Wang^{2,5} Chenglu Wen¹ ✓ Xiamen University ² Zhongguancun Academy ³ Nanyang Technological University ⁴ University of Chinese Academy of Sciences ⁵ Beihang University

huangxun@stu.xmu.edu.cn, weixinli@buaa.edu.cn, clwen@xmu.edu.cn

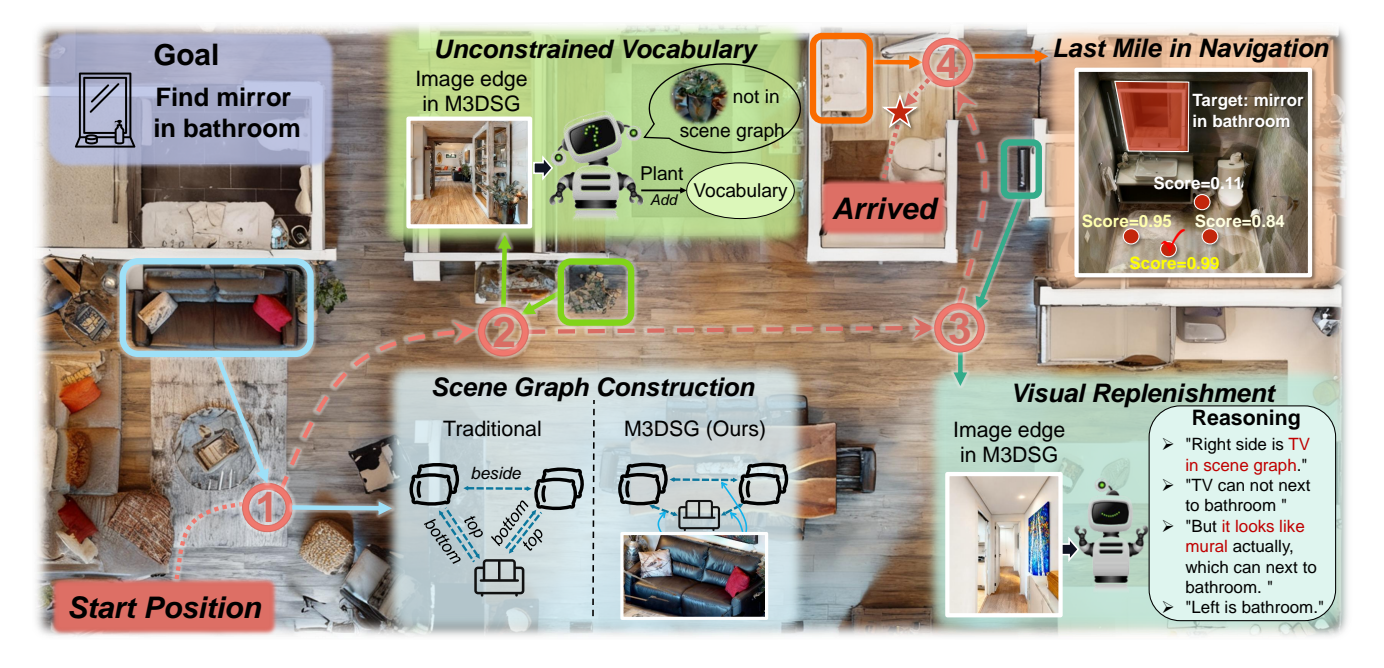


Figure 1. One example illustrating the key insights of our work. We introduce the Multi-modal 3D Scene Graph (M3DSG) as an alternative to traditional 3D scene graphs, enabling efficient scene graph generation. By incorporating dynamically preserved image-edge information, M3DSG supports unconstrained vocabulary and enhanced visual replenishment for the agent, thereby allowing more comprehensive and context-aware scene understanding in navigation tasks. Furthermore, to address the last-mile problem of selecting the optimal navigation viewpoint given a target location, we propose a visibility-based scoring mechanism for candidate viewpoints.

Abstract

Embodied navigation is a fundamental capability for robotic agents operating. Real-world deployment requires open vocabulary generalization and low training overhead, motivating zero-shot methods rather than task-specific RL training. However, existing zero-shot methods that build explicit 3D scene graphs often compress rich visual observations into text-only relations, leading to high construction cost, irreversible loss of visual evidence, and constrained vocabularies. To address these limitations, we introduce the Multi-modal 3D Scene Graph (M3DSG), which preserves visual cues by replacing textual relational edges with

dynamically assigned images. Built on M3DSG, we propose MSGNav, a zero-shot navigation system that includes a Key Subgraph Selection module for efficient reasoning, an Adaptive Vocabulary Update module for open vocabulary support, and a Closed-Loop Reasoning module for accurate exploration reasoning. Additionally, we further identify the "last mile" problem in zero-shot navigation — determining the feasible target location with a suitable final viewpoint, and propose a Visibility-based Viewpoint Decision module to explicitly resolve it. Comprehensive experimental results demonstrate that MSGNav achieves state-of-the-art performance on GOAT-Bench and HM3D-OVON datasets. The open-source code will be publicly available at here.

1. Introduction

Embodied navigation is a fundamental capability of robotic agents, enabling them to accomplish diverse tasks in realistic environments [47, 51]. Such tasks are typically goaloriented, with targets defined by objects, natural language descriptions, or images [45]. Recently, the challenging open-vocabulary embodied navigation task [54] has gained increasing attention, as real-world agents are required to generalize to a wide and unconstrained range of object categories [47].

Previous RL-based embodied navigation methods [27, 35] suffer from poor generalization and a large sim-to-real gap [44]. Inspired by rapid advances in pre-trained large model techniques [1, 14], zero-shot embodied navigation approaches have emerged at this historic moment. Zero-shot navigation system does not require any training or fine-tuning before being applied to real-world scenarios. These approaches [15, 43, 48, 55] substantially reduce training time and computational cost while enabling open-vocabulary navigation, thereby facilitating deployment in real-world applications.

Notably, a series of methods [30, 38, 39] that build explicit 3D scene graphs from observations and leverage LLMs to drive exploration have shown promising performance on standard goal-oriented navigation benchmarks [2, 31]. However, traditional 3D scene graphs overly abstract 3D object relations into simple textual labels (e.g., "top", "beside"), which seriously impedes progress on zeroshot embodied navigation. As illustrated in Fig. 1, the extreme abstracted 3D object-relation in traditional 3D scene graphs introduces three main limitations:

- **X** Expensive Construction. Traditional 3D scene graphs rely on frequent MLLM queries for relation inference, incurring substantial token and time overhead.
- **X** Visual Deficiency. Converting visual observations into text-only graphs discards visual evidence, leading to ambiguity and sensitivity against perception errors.
- ✗ Constrained Vocabulary. Novel categories beyond a preset vocabulary cannot be represented, limiting generalization in 3D scene graph-based methods.

Based on these observations, we conclude that visual information is indispensable to the real-world navigation process. Therefore, as illustrated in Fig. 1, we introduce the Multi-modal 3D Scene Graph (M3DSG), which replaces the pure-text relational edges with dynamically assigned images to incorporate visual cues, and facilitates efficient and open-vocabulary inference. Specifically, our M3DSG effectively addresses the three limitations above:

✓ Efficient Construction: M3DSG eliminates costly MLLM queries, greatly reducing construction overhead.

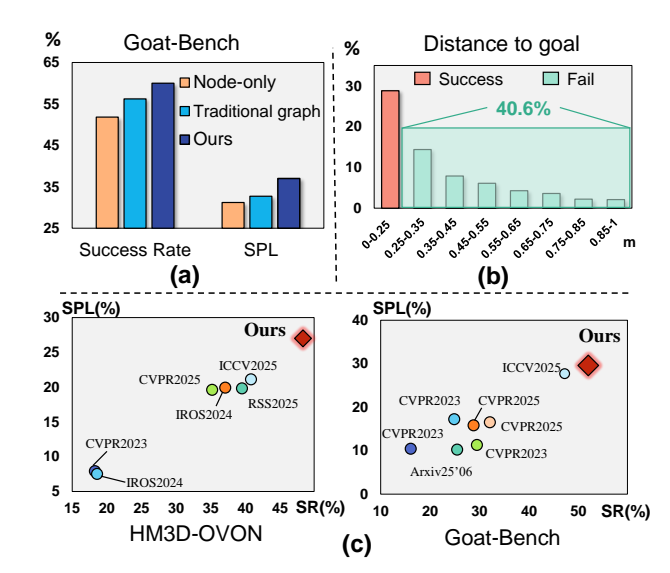


Figure 2. Performance comparisons between our method and other existing ones for embodied navigation. (a) The superiority of our M3DSG over traditional 3D scene graphs. (b) Distance statistics from the goal for the previous method (3D-Mem [43] as an example). (c) Our MSGNav system achieves state-of-the-art performance on both HM3D-OVON and Goat-Bench benchmarks.

- ✓ Visual Replenishment: M3DSG provides visual contexts to enhance robustness against perception errors.
- ✓ Unconstrained Vocabulary: M3DSG utilizes preserved visual contexts to expand vocabulary, enabling openvocabulary generalization dynamically.

As shown in Fig. 2(a), our M3DSG markedly outperforms traditional text-only 3D scene graphs in the zero-shot embodied navigation task. Building on M3DSG, we further propose MSGNav, a navigation system that unleashes the power of Multi-modal 3D Scene Graph for zero-shot embodied Navigation. As illustrated in Fig. 1, MSGNav first selects target-relevant subgraphs from the complex multi-modal 3D scene graph by a key-subgraph selection module. During the exploration process, MSGNav updates the vocabulary using preserved visual information and incorporates a closed-loop reasoning module for accurate exploration reasoning, thereby enabling unconstrained vocabulary and reliable navigation.

Additionally, we realize that the *last-mile* problem in navigation tasks — knowing the target's location is not equivalent to determining a suitable navigation pose¹. Existing zero-shot embodied navigation methods usually stop before that final step. As shown in Fig. 2(b), the existing 3D-Mem method [43] successfully approaches the target but still fails in many navigation tasks due to unacceptable viewpoints (distances ranging from 0.25 m to 1.0 m).

¹Cannot see the wood for the trees. Being too close or occluded prevents a clear observation of the target, which is not a good viewpoint.

 [□] Corresponding author.

To address this issue, we introduce a visibility-based view-point decision module in our MSGNav.

As shown in Fig. 2(c), MSGNav significantly outperforms state-of-the-art RL-based and zero-shot methods on the Val-Unseen set of challenging embodied navigation GOAT-Bench [16] and HM3D-OVON [47], demonstrating consistent and substantial gains in zero-shot embodied navigation. Our contributions can be summarized as follows:

- M3DSG: We propose a multi-modal 3D scene graph that incorporates visual information, overcoming pure-text limitations and enhancing open-vocabulary scene representation for embodied navigation.
- Last-Mile: We identify the last-mile problem and propose a visibility-based viewpoint decision module to address it.
- MSGNav: We develop a zero-shot embodied navigation system built on M3DSG, enabling active exploration and achieving state-of-the-art performance on the GOAT-Bench and HM3D-OVON embodied navigation datasets.

2. Related Work

2.1. Graph-based Scene Exploration

Graph representations [11, 17, 37] provide explicit spatial–semantic structures for scene reasoning and integrate well with LLMs/VLMs. Examples include SayPlan [36] for 3D scene graph planning, OVSG [3] for open-vocabulary grounding, imaginative world modeling [13], and BEV graph policies [26]. Graph reasoning has also been applied in navigation, e.g. SG-Nav [44] for hierarchical prompting and graph-retained adaptation [12] for cross-domain VLN. Yet, the overly abstract textual edges of current scene graphs limit the comprehensive scene context understanding, motivating our multi-modal 3D scene graph (M3DSG).

2.2. Zero-Shot Navigation

Previous embodied navigation methods, primarily based on reinforcement learning (RL) [27, 35], suffer from limited generalization and a significant sim-to-real gap, which hinders their application in real-world environments. Zeroshot navigation allows agents to act in unseen environments without task-specific training, unlike supervised methods [8, 20, 32, 41] which require large-scale simulation. Existing zero-shot navigation methods span object-goal (ON), image-goal (IIN), and text-goal (TN). ON methods include CoW [9] with CLIP [29] frontier exploration, ESC [53], OpenFMNav [4], VLFM [46] using LLM reasoning, UniGoal [45] for multi-modal unification, and RATE-Nav [22] with region-aware termination. IIN methods range from Mod-IIN [19] to SIGN [42] for safety-aware drone navigation. TN methods such as InstructNav [24] generalize instruction following across ON, DDN, and VLN [5, 21, 25, 49, 52]. However, most zero-shot work ignores the last-mile challenge of choosing an optimal viewpoint after target localization.

3. Approach

In this section, we formalize the zero-shot goal-oriented embodied navigation problem and provide an overview of our pipeline (Sec. 3.1). We then introduce the proposed Multi-modal 3D Scene Graph (M3DSG) (Sec. 3.2), and describe MSGNav, the navigation system built on M3DSG (Sec. 3.3).

3.1. Zero-shot Goal-Oriented Embodied Navigation

3.1.1. Problem definition

We consider a mobile embodied agent operating in an unknown or partially explored environment (i.e. the lifelong navigation setting). The agent receives target information in the form of an category, natural language description, or reference image. At each time step t, it obtains an RGB-D observation \mathcal{I}_t and executes an action \mathcal{A}_t (camera rotation or ego-motion) to actively explore until locating the target. The task is successful if the agent reaches any target viewpoint within d meters in at most T steps; otherwise, it fails. In the zero-shot navigation setting, the agent performs navigation without task-specific training or fine-tuning in simulation, thereby reducing training cost and improving generalization to unseen environments and targets.

3.1.2. Overview

Zero-shot goal-oriented embodied navigation remains highly challenging for conventional learning-based methods. Following current best practices, we utilize off-the-shelf pre-trained models: Vision Foundation Models (VFMs) and Vision Language Models (VLMs) for primitive reasoning. While these models excel in visual understanding, they are limited in 3D spatial reasoning. To address this gap, we propose the M3DSG, an explicit and multimodal 3D scene graph that is incrementally built to encode scene contexts while preserving the visual evidence. Based on M3DSG, the navigation system MSGNav completes goal-oriented navigation with a Visibility-based Viewpoint Decision (VVD) module.

Formally, at each time step t, M3DSG incrementally integrates the RGB-D observation \mathcal{I}_t into an evolving scene graph \mathbf{S} . MSGNav then uses \mathbf{S} as a prompt to guide VLMs in locating candidate target \bar{o} positions or unexplored frontier for exploration. Finally, the VVD module selects an optimal navigation viewpoint \mathbf{v}_{best} with the best line of sight to \bar{o} , enabling a successful final approach to the target.

3.2. M3DSG: Multi-modal 3D Scene Graph

Traditional 3D scene graphs represent object relations with text-only edges, which are overly abstract and hinder VLMs from accurately understanding scene contexts. Inspired by

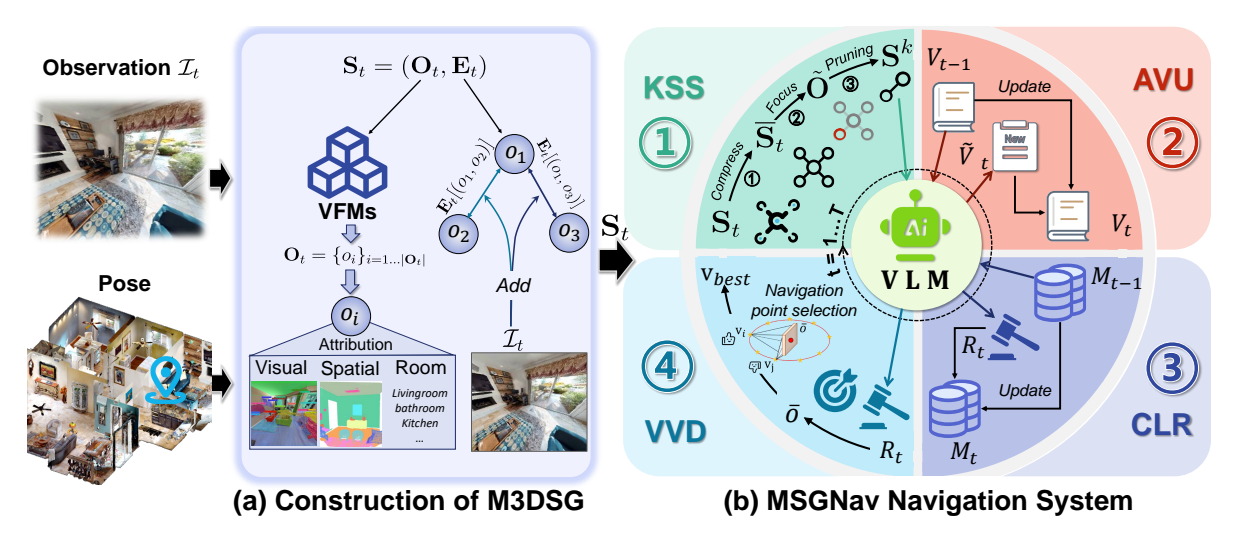


Figure 3. The overall framework of our MSGNav. At time step t, the agent incrementally constructs the scene graph S_t based on received observation \mathcal{I}_t and its own pose. S_t includes a set of objects \mathbf{O}_t with attributes, namely visual, spatial, and room properties, along with a set of image edges \mathbf{E}_t representing object relationships. Subsequently, S_t is processed through KSS, AVU, and CLR modules, before being input to VLM query to obtain the target object \bar{o} . Finally, VVD module selects the insightful viewpoint \mathbf{v}_{best} as a navigation point.

3D-Mem [43], which emphasizes the value of raw images for navigation, we retain visual information when constructing an object-centric 3D scene graph. Unlike traditional 3D scene graph [11] which uses textual relation edges, our method stores images to describe detailed object relations directly. This image edge preserves the benefits of 3D scene graphs while avoiding repeated, costly model queries and providing a more holistic scene representation.

To mitigate the inference cost of numerous images during exploration, we design a dynamic allocation algorithm that efficiently converts the multimodal 3D scene graph into prompts, thereby requiring on average only **4 images** per query to represent the target-related scene context.

3.2.1. M3DSG Structure Definition

During the environment exploring process, M3DSG constructs a scene graph $\mathbf{S} = (\mathbf{O}, \mathbf{E})$, where $\mathbf{O} = \{o_i\}_{i=1}^{N_o}$ and $\mathbf{E} = \{\mathbf{e}_j\}_{j=1}^{N_e}$ denote the sets of objects and edges, respectively. Here, N_o is the number of detected objects, and $N_e = \sum_{1 \leq x < y \leq N_o} \mathbb{1}_{\|Pos_{o_x} - Pos_{o_y}\| < \theta}$ is the number of object pairs (o_x, o_y) whose spatial distance is below θ . Each object o_i is described by attributes including corresponding category, 3D coordinates, and room locations. Each edge \mathbf{e}_j stores a set of RGB-D images $\mathbf{I}_j = \{\mathcal{I}_k\}_{k=1}^{|\mathbf{I}_j|}$ that represent the pair of corresponding objects to record their visual relationship.

3.2.2. Incremental Construction of M3DSG

Following prior work [44, 45], the scene graph S is incrementally updated during exploration. At step t, S_{t-1} is updated to S_t with the current RGB-D observation \mathcal{I}_t as:

$$\mathbf{S}_t = \mathcal{M}(\mathbf{S}_{t-1}, \mathcal{I}_t), \quad t \in [1, T], \quad \mathbf{S}_0 = (\varnothing, \varnothing), \quad (1)$$

where \mathcal{M} is the graph update function consisting of Object \mathbf{O}_t Update and Edge \mathbf{E}_t Update.

Object Update. For the RGB-D observation \mathcal{I}_t at time t, we extract the frame-level object set $\mathbf{O}_t^{frame} = \{o_i\}_{i=1}^{|\mathbf{O}_t^{frame}|}$ by VFMs: YOLO-W [6] for open-vocabulary detection, SAM [18] for instance masks, and CLIP [28] for visual embeddings. Each object o_i is represented as $o_i = \{\mathcal{ID}, \mathcal{C}, \mathcal{P}, \mathcal{B}, \mathcal{M}, \mathcal{PC}, \mathcal{V}, \mathcal{R}\}_i$, denoting unique ID, category, 3D position, bounding box, semantic mask, point cloud, visual feature, and room location, respectively. The global object set \mathbf{O}_t is incrementally updated from the previous set \mathbf{O}_{t-1} and the frame-level object set \mathbf{O}_t^{frame} as:

$$\mathbf{O}_t = \Phi_{\text{merge}} (\Phi_{\text{match}}(\mathbf{O}_t^{frame}, \mathbf{O}_{t-1})) \cup \mathbf{O}_t^{frame}, \quad (2)$$

where Φ_{match} aligns objects in \mathbf{O}_t^{frame} and \mathbf{O}_{t-1} via spatial similarity $(\mathcal{B},\mathcal{PC})$ and visual similarity $(\mathcal{C},\mathcal{V})$, and Φ_{merge} merges features of matched objects [11]. This process maintains a global object set \mathbf{O}_t within \mathbf{S}_t step by step. **Edge Update**. The core of an edge is a set of images \mathbf{I} in which an object pair co-occurs, indexed by the unique IDs of the object pair, *i.e.* $\mathbf{E}: (\mathcal{ID}, \mathcal{ID}) \to \mathbf{I}$.

Meanwhile, we maintain a mapping from each image to its corresponding object pair, *i.e.* $\mathbf{H} : \mathcal{I} \to (\mathcal{ID}, \mathcal{ID})$.

For the current RGB-D frame \mathcal{I}_t at step t with object set \mathbf{O}_t^{frame} (from Object Update), we generate co-occurring object pairs (o_x, o_y) that appear together in \mathcal{I}_t as:

$$\{(o_x, o_y) \in \mathbf{O}_t^{frame} \times \mathbf{O}_t^{frame} \mid o_x \neq o_y \land \|\mathcal{P}_{o_x} - \mathcal{P}_{o_y}\| \leq \theta\},\$$
(3)

where θ is the adjacency distance threshold. The edge set \mathbf{E}_t is then updated by retrieving the unique IDs $(\mathcal{ID}_{o_x}, \mathcal{ID}_{o_y})$ of each detected pair and appending \mathcal{I}_t to the corresponding image set as:

$$\begin{split} \mathbf{E}_{t}[(\mathcal{I}\mathcal{D}_{o_{x}},\mathcal{I}\mathcal{D}_{o_{y}})] \leftarrow \begin{cases} \{\mathcal{I}_{t}\} & \text{if } (\mathcal{I}\mathcal{D}_{o_{x}},\mathcal{I}\mathcal{D}_{o_{y}}) \notin \text{dom}(\mathbf{E}_{t-1}) \\ \mathbf{E}_{t-1}[(\mathcal{I}\mathcal{D}_{o_{x}},\mathcal{I}\mathcal{D}_{o_{y}})] \cup \{\mathcal{I}_{t}\} & \text{otherwise} \end{cases} \\ \mathbf{H}[\mathcal{I}_{t}] \leftarrow \begin{cases} \{(\mathcal{I}\mathcal{D}_{o_{x}},\mathcal{I}\mathcal{D}_{o_{y}})\} & \text{if } \mathcal{I}_{t} \notin \text{dom}(\mathbf{H}) \\ \mathbf{H}[\mathcal{I}_{t}] \cup (\mathcal{I}\mathcal{D}_{o_{x}},\mathcal{I}\mathcal{D}_{o_{y}}). & \text{otherwise} \end{cases} , \\ \text{dom}(X) = \{k \mid \exists v : (k,v) \in X\}. \end{cases} \tag{4}$$

This edge update process is efficient, eliminating the need for costly VLM queries. Moreover, the stored image recorded in \mathbf{E}_t provides compact and visually grounded representations of object relationships, which can be directly utilized for downstream exploration reasoning.

3.3. MSGNav Embodied Navigation System

M3DSG provides comprehensive scene representations that preserve rich visual information. To fully exploit this, we propose the navigation system MSGNav. As shown in Fig. 3(b), our MSGNav first significantly reduces the tokens and time cost required for inference by selecting key subgraphs (Sec. 3.3.1). MSGNav then addresses the out-of-vocabulary issue inherent to pre-set vocabulary by adaptively updating vocabulary with visual evidence from M3DSG (Sec. 3.3.2). Meanwhile, MSGNav performs closed-loop reasoning via decision memory and feedback (Sec. 3.3.3). Finally, MSGNav tackles the "last-mile" problem by optimizing navigation points through visibility-based viewpoint decisions (Sec. 3.3.4).

3.3.1. Key Subgraph Selection (KSS)

During exploration, the 3D scene graph **S** grows progressively and can become voluminous, thereby impairing the decision-making efficiency [43]. In embodied navigation, however, typically only a small related subgraph to the required target is meaningful. Therefore, processing the full scene graph consumes substantial computational resources without commensurate benefits. The key to addressing this issue is to preserve maximal relevant information with the minimal scene graph. MGSNav extracts the target-relevant subgraphs via a **Compress–Focus–Prune** procedure:

- Compress. We first simplify the rich but vast scene graph \mathbf{S} into the compact adjacency list representation $\hat{\mathbf{S}} = (\hat{\mathbf{O}}, \hat{\mathbf{E}})$. For each object $\hat{o}_i \in \hat{\mathbf{O}}$, we retain only essential attributes (ID and category): $\hat{o}_i = \{\mathcal{ID}, \mathcal{C}\}_i$. The edge set is represented as undirected adjacency list: $\hat{\mathbf{E}}_{\hat{o}_i} = \{ID_{\hat{o}_i}|\hat{o}_i \in \hat{\mathbf{O}}, (ID_{\hat{o}_i}, ID_{\hat{o}_i}) \in dom(E)\}$.
- Focus. The compressed scene graph $\hat{\mathbf{S}}$ significantly reduces the overhead. Therefore, we directly fed it to the VLM to select top-k related objects $\mathbf{O}^{rel} \subset \mathbf{O}$ which are the most relevant to the current navigation target.
- **Pruning.** Finally, we construct the key subgraph $S^k = (O^k, E^k)$ by progressively selecting the image that covers the most edges through a dynamic greedy allocation algorithm (in Algorithm 1).

The selected key subgraph S^k is used to query the VLM

Algorithm 1 Greedy Dynamic Allocation for Pruning

```
Require: Image-Object Association Map: H
       Scene Graph: S = (O, E), Related Objects: O^{rel}
  1: \mathbf{E}^k \leftarrow \varnothing
                                                                                        2: \mathbf{O}^k \leftarrow \mathbf{O}^{rel}
                                                                                      ▶ Key objects
  3: \mathbf{U} \leftarrow \varnothing
                                                               4: \mathbf{I}^{total} \leftarrow \emptyset
                                                                                    5: for o \in \mathbf{O} do
                                                                     ⊳ Filter relevant edges
              if \exists o^r \in \mathbf{O}^{rel}: (\mathcal{ID}_o, \mathcal{ID}_{o^r}) \in \text{dom}(\mathbf{E}) then
                     \mathbf{O}^k \leftarrow \mathbf{O}^k \cup o
  7:
                      \begin{array}{l} \mathbf{U} \leftarrow \mathbf{U} \cup (\mathcal{ID}_o, \mathcal{ID}_{o^r}) \\ \mathbf{I}^{total} \leftarrow \mathbf{I}^{total} \cup \mathbf{E}[(\mathcal{ID}_o, \mathcal{ID}_{o^r})] \end{array} 
  8:
  9:
 10:
11: end for
      while U \neq \emptyset do
                                                                            \mathcal{I}^{\star} \leftarrow \arg \max_{\mathcal{I} \in \mathbf{I}^{total}} |\mathbf{H}[\mathcal{I}] \cap \mathbf{U}|
14:
               \mathbf{E}^k[\mathbf{H}[\mathcal{I}^{\star}] \cap \mathbf{U}] \leftarrow \mathcal{I}^{\star} \quad \triangleright \mathcal{I}^{\star} cover the most edges.
               \mathbf{U} \leftarrow \mathbf{U} \setminus \mathbf{H}[\mathcal{I}^{\star}]
                                                                16: end while
17: return S<sup>k</sup> = (\mathbf{O}^k, \mathbf{E}^k)
```

for exploratory reasoning with low cost (on average \sim 4 images per query):

$$\mathcal{R}_t = \text{VLM}(\mathbf{S}^k, \mathbf{F}, g, t), \tag{5}$$

where \mathbf{F} denotes frontier images for exploration as in [43], g is the navigation target, and \mathcal{R}_t denotes the selected target or frontier for task response. The specific prompt design is provided in the supplementary material.

This technique reduces the token cost by over 95% while feeding the information to VLM for reasoning, retaining most of the important objects relevant to the task. Consequently, the agent can efficiently focus on task-relevant entities, improving both navigation speed and performance.

3.3.2. Adaptive Vocabulary Update (AVU)

Existing methods achieve open-vocabulary navigation simply by using detectors, e.g., YOLO-W [6] and GroundingDINO [23], but remain constrained by preset vocabulary (e.g., ScanNet-200 [7], HM3D [31]). Such constraints hinder VLMs from handling diverse out-of-vocabulary scene representations in the real world. Additionally, preset vocabulary is difficult to accurately describe the image target.

To address this issue, MSGNav integrates adaptive vocabulary updates with preserved visual evidence during the exploratory reasoning process. We first initialize the vocabulary $V_{t=0}$ with the ScanNet-200. During exploration at time t, the VLM inspects edge images \mathbf{E}_t and compares objects in \mathbf{O}_t to propose required novel vocabulary \hat{V}_t (based on the extension of Eq. 5):

$$\mathcal{R}_t, \hat{V}_t = \text{VLM}(\mathbf{S}^k, \mathbf{F}, q, t). \tag{6}$$

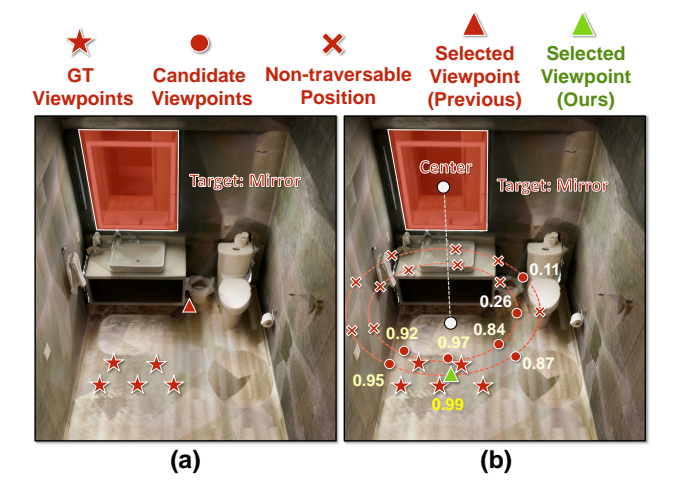


Figure 4. Demonstration of the "last-mile" problem. (a) Previous methods select the nearest traversable position after target localization, and often fail due to poor or distant viewpoints. (b) Our VVD samples candidate viewpoints and computes visibility, and is able to select a suitable viewpoint close to the ground-truth (GT) viewpoint for successful navigation.

Then the novel vocabulary \hat{V} will be incorporated into V_t : $V_t = V_{t-1} \cup \hat{V}_t$. By continuously updating vocabulary V_t in this manner, the scene graph progressively captures richer and more accurate object descriptions, supporting navigation beyond preset vocabulary limitations.

3.3.3. Closed-Loop Reasoning (CLR)

Memory is critical for navigation agents. While prior work focuses mainly on scene memory, other forms of memory can also influence decision-making. In addition to modeling the scene as perception memory, we introduce the *decision memory* \mathbf{M} for closed-loop reasoning. At time step t-1, the exploration response \mathcal{R}_{t-1} is stored in a historical action repository \mathbf{M}_t as $\mathbf{M}_t = \mathbf{M}_{t-1} \cup \mathcal{R}_t$, $\mathbf{M}_0 = \varnothing$. Then \mathbf{M}_t is utilized at time step t to assist subsequent decisions (based on the extension of Eq. 6) as:

$$\mathcal{R}_t, \hat{V}_t = \text{VLM}(\mathbf{S}^k, \mathbf{M}_t, \mathbf{F}, g, t). \tag{7}$$

This closed-loop reasoning enhances the accuracy of VLM strategies by memorizing past decision feedback to inform current decisions.

3.3.4. Visibility-based Viewpoint Decision (VVD)

For a navigation agent, its high-level decision process involves the selection of a target coordinate, while the low-level planner converts it into executable actions. Therefore, an optimal final decision should choose a viewpoint with clear visibility to facilitate subsequent operations. Previous zero-shot methods [10, 15, 43, 44] often assume that knowing the target location is enough, and select the nearest traversable position as the navigation viewpoint. However,

as shown in Fig. 4(a), this may yield navigation viewpoints with occlusion or poor visibility, causing failure even when the target \bar{o} is correctly localized.

We term this the "last-mile" problem of navigation—identifying a suitable viewpoint despite correctly locating the target \bar{o} . To solve this problem, we realize that a good viewpoint should have clear visibility of the target. To achieve this goal, we propose a *Visibility-based Viewpoint Decision* (VVD) module (in Algorithm 2). As shown in Fig. 4(b), VVD uniformly samples candidate viewpoints around target \bar{o} within radii $\mathbf{R} = \{r_j\}_{j=1}^{N_R}$. For each candidate \mathbf{v}_i , VVD computes a visibility score by evaluating occlusion between \mathbf{v}_i and target point cloud $\mathcal{PC}_{\bar{o}}$. The viewpoint with the highest visibility score \mathbf{v}_{best} is selected as the navigation coordinate. Compared with traditional nearest-point choice, VVD consistently yields viewpoints with superior target visibility.

Algorithm 2 Visibility-based Viewpoint Decision

Require: Target object \bar{o} , Scene point cloud \mathcal{PC} , Radii set \mathbf{R} , Samples number K, Camera height h, Obstruction distance τ 1: $\mathbf{c}_{\bar{o}} \leftarrow \frac{1}{|\mathcal{PC}_{\bar{o}}|} \sum_{\mathbf{p} \in \mathcal{PC}_{\bar{o}}} \mathbf{p}$ \triangleright Target center 2: $\Theta \leftarrow \left\{ \frac{2\pi k}{K} \mid k = 0, \dots, K - 1 \right\}$ \triangleright Sampling angles 3: $\mathbf{V}_c \leftarrow \bigcup_{r_i \in \mathbf{R}} \left\{ \mathbf{c}_{\bar{o}} + [r_i \cos \theta, h - \mathbf{c}_{\bar{o}}[1], r_i \sin \theta] \mid \theta \in \Theta \right\}$ 4: $\mathbf{V}_c \leftarrow \left\{ \mathbf{v} \in \mathbf{V}_c \mid \mathbf{v} \text{ is traversable} \right\}$ \triangleright Candidate viewpoints 5: $S_{best} \leftarrow 0, \mathbf{v}_{best} \leftarrow \mathbf{0}$ ▶ Initialization 6: for each $\mathbf{v}_i \in \mathbf{V}_c$ do
$$\begin{split} & \mathcal{Q}(\mathbf{v}_i, \mathbf{p}) = \left\{ \mathbf{v}_i + t \cdot \frac{\mathbf{p} - \mathbf{v}_i}{\|\mathbf{p} - \mathbf{v}_i\|} \, \middle| \, t \in [\tau, \|\mathbf{p} - \mathbf{v}_i\| - \tau] \right\} \\ & \mathcal{E}(\mathbf{v}_i, \mathbf{p}) = \forall \mathbf{q} \in \mathcal{Q}(\mathbf{v}_i, \mathbf{p}) : \min_{\mathbf{s} \in \mathcal{PC}} \|\mathbf{q} - \mathbf{s}\| \geq \tau \\ & S_{\mathbf{v}_i} \leftarrow \frac{1}{|\mathcal{PC}_{\bar{o}}|} \sum_{\mathbf{p} \in \mathcal{PC}_{\bar{o}}} \mathbb{1}_{\mathcal{E}(\mathbf{v}_i, \mathbf{p})} \quad \triangleright \text{ Visibility ratio} \\ & \text{if } S_{\mathbf{v}_i} > S_{best} \text{ then} \end{split}$$
10: $S_{best} \leftarrow S_{\mathbf{v}_i}, \mathbf{v}_{best} \leftarrow \mathbf{v}_i$ 11: 12: end if 13: end for 14: return \mathbf{v}_{best} ▶ Best viewpoint maximizing visibility

4. Experiment

4.1. Experimental Setting

We evaluate on two goal-oriented open-vocabulary navigation benchmarks: HM3D-OVON [47] (open-vocabulary navigation), and GOAT-Bench [16] (multi-modal lifelong open-vocabulary navigation). The metric of navigation task includes Success Rate (SR = $\frac{N_{\text{Success}}}{N_{\text{total}}}$) and Success Path Length (SPL = $\frac{1}{N_{\text{total}}}\sum_{i=1}^{N_{\text{total}}}S_i\frac{l_i^s}{\max(l_i^s,l_i^a)}$), where $S_i \in \{0,1\}$ indicates success of task, l_i^s and l_i^a represent shortest path length and agent path length, respectively. To demonstrate generalization capabilities, we evaluate approaches on the " $Val\ Unseen$ " set of GOAT-Bench and HM3D-OVON datasets. We adopt GPT-40 (2024-08-06 version) as the choice of VLM by directly utilizing the OpenAI API. We also provide results using Owen-VL-Max (2025-08-13 version)

sion) as the choice of VLM in the Appendix.

4.2. Main Experimental Results

We will show the main comparison results with other stateof-the-art methods on the Goat-Bench and OVON datasets. For clarity, we report only the primary results here, and detailed results will be provided in the Appendix.

4.2.1. HM3D-OVON

Method	Training-free	SR↑	SPL ↑
BCRL [33]	×	8.0	2.5
DAgger [34]	×	10.2	4.7
DAgRL [34]	×	18.3	7.9
RL [40]	×	18.6	7.5
VLFM [46]	\checkmark	35.2	19.6
Uni-NaVid [50]	×	39.5	19.8
TANGO [55]	\checkmark	35.5	19.5
DAgRL+OD [47]	×	37.1	19.9
MTU3D [54]	×	40.8	12.1
MSGNav (Ours)	✓	48.3	27.0

Table 1. Experiments on the "Val Unseen" split of HM3D-OVON.

Table 1 demonstrates that our proposed MSGNav significantly outperforms all other methods on both SR and SPL metrics in open-vocabulary navigation. Notably, while achieving the highest SR of 48.3%, MSGNav also exhibits an exceptionally high SPL, surpassing the previous state-of-the-art training-based method MTU3D [54] by 7.5% in SR and 14.9% in SPL. This shows that our approach effectively balances accuracy and efficiency in the navigation exploration process for unseen scenarios.

4.2.2. Goat-Bench

The results in Table 2 also show the outstanding performance of our MSGNav in tackling multimodal goals, lifelong navigation task settings. MSGNav achieves the best performance with 52.0% SPL and 29.6% SPL compared to both previously training-based and train-free methods. It surpasses the previous state-of-the-art training-based method MTU3D [54] by 4.8% SR and 2.1% SPL, demonstrating its superior navigation capabilities. These results highlight the effectiveness of our multi-modal scene graph in tackling multi-modal lifelong navigation tasks.

4.3. Ablation Analysis

In this section, we further analyze the effectiveness and advancement of each module in the MSGNav system. Specifically, this includes component ablation, the advantages of multimodal edges, and demonstrating how the VVD module aids in "last-mile" decision-making.

Method	Training-free	SR ↑	SPL ↑
SenseAct-NN Monolitic [16]	×	12.3	6.8
Modular CLIP on Wheels [16]	\checkmark	16.1	10.4
Modular GOAT [16]	✓	24.9	17.2
SenseAct-NN Skill Chain [16]	×	29.5	11.3
VLMnav [10]	✓	20.1	9.6
DyNaVLM [15]	✓	25.5	10.2
3D-Mem [†] [43]	✓	28.8	15.8
TANGO [55]	✓	32.1	16.5
MTU3D [54]	×	47.2	27.7
MSGNav (Ours)	✓	52.0	29.6

Table 2. Experiments on the "Val Unseen" split of GOAT-Bench. "†" denotes the results we reproduced due to different settings.

4.3.1. Effective of Component

Table 3 demonstrates the impact of each component. Firstly, introducing MSG3D yielded an improvement of 15.0% in SR and 7.8% in SPL (row 2). Subsequently, VVD further gains 12.5% in SR and 6.7% in SPL (row 3). Notably, introducing either AVU (row 4) or CLR (row 5) alone can only improve a part of categories. This is because AVU's new vocabulary may introduce some insufficient perception results, while the strict decision-making of CLR may hinder navigation toward detailed language-described targets. However, the optimal performance of simultaneously incorporating AVU and CLR (row 6) shows that AVU and CLR are complementary. AVU can supplement extra perception information for the strict decision-making of CLR, while CLR can address the insufficient perception of AVU. These results validate the effectiveness of each component.

4.3.2. Advantage of M3DSG

Table 4 shows the experimental results comparing MSGNav using Node-only, Concept-graph [11], and our M3DSG. Concept-graph outperforms Node-only by 4.4% in SR and 1.5% in SPL, especially for Language and Image goals, underscoring the value of relationship edges. M3DSG further boosts these categories with a total of 3.8% SR and 4.3% SPL, showing its effectiveness in scene understanding. It is worth noting that node-only performs well on category goals, mainly because such tasks rely on concise object sets rather than complex contextual information.

4.3.3. Decision-making for "Last-mile"

Table 5 validates the effectiveness of VVD in addressing the "last-mile" problem. Navigating without VVD yields only a 33.91% SR at the standard threshold of d = 0.25 m. As the threshold is relaxed, its SR can be significantly improved, indicating that lots of failed tasks stop near the target due to incorrect navigation point selection. Navigating with VVD can improve SR to 51.91%, which primarily recovers

	Modu	ıle		Success Rate				SPL			
M3DSG	VVD	AVU	CLR	Overall	Category	Language	Image	Overall	Category	Language	Image
				28.8	29.9	26.8	29.5	20.2	21.0	18.7	21.0
\checkmark				43.8	56.0	35.1	40.2	28.0	31.3	23.5	29.1
\checkmark	\checkmark			56.3	61.6	55.0	52.3	34.7	34.9	33.9	35.2
\checkmark	\checkmark	\checkmark		55.3	58.6	51.7	55.7	36.7	35.3	34.8	40.1
\checkmark	\checkmark		\checkmark	53.2	64.6	38.5	55.7	32.9	34.8	25.8	37.7
\checkmark	\checkmark	\checkmark	\checkmark	60.0	63.6	57.2	59.1	37.0	35.0	33.4	42.6

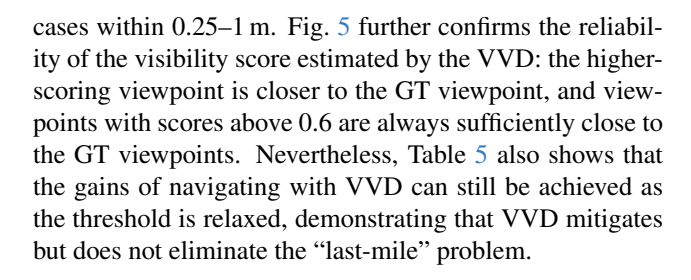
Table 3. Component ablation experiment across the first episode of each scene on the "Val Unseen" split of GOAT-Bench. The first row without any module, which represents our baseline model 3D-Mem [43] results. "VVD", "AVU", and "CRV" represent the Visibility-based Viewpoint Decision module, Adaptive Vocabulary Update module, and Closed-loop Reasoning and Verification module.

3D Scene Graph		Succes	s Rate		SPL			
3D Scelle Graph	Overall	Category	Language	Image	Overall	Category	Language	Image
Node-only	51.8	63.6	44.0	47.8	31.2	39.3	20.5	33.8
Traditional graph [11]	56.2	63.6	52.8	52.3	32.7	35.3	27.3	35.5
M3DSG (Ours)	60.0	63.6	57.2	59.1	37.0	35.0	33.4	42.6

Table 4. Scene graph experiment across the first episode of each scene on the "*Val Unseen*" split of GOAT-Bench. "Node-only" indicates Concept-graph [11] without object relation edges. "Traditional graph" indicates Concept-graph [11].

Success Threshold	Success Rate (MSGNav)				
$d(\mathbf{m})$	w/o VVD	w/ VVD			
0.25 (standard)	33.91	51.97			
0.35	48.93	59.69			
0.45	54.59	61.73			
0.55	57.44	63.03			
0.65	59.65	63.78			
0.75	60.40	64.52			
0.85	61.30	65.22			
1.00	62.38	66.52			

Table 5. Experiments on the "Val Unseen" split of GOAT-Bench with various success thresholds. VVD module represents the Visibility-based Viewpoint Decision module.



5. Conclusion

In this paper, we propose the MSGNav, a zero-shot embodied navigation framework built upon a Multi-modal 3D Scene Graph (M3DSG) that preserves visual information for efficient construction, robust perception, and

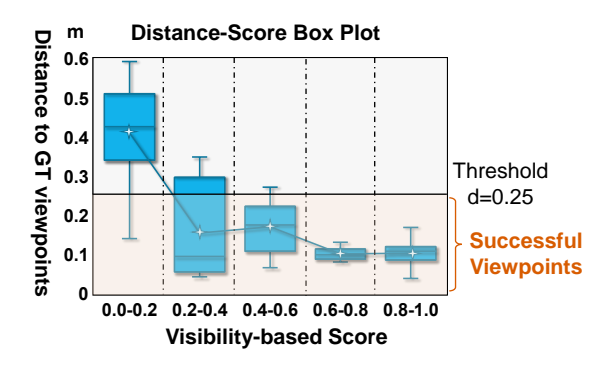


Figure 5. Statistical box plot of candidate viewpoint scores computed by the VVD module and distances from GT viewpoints.

unconstrained vocabulary. Meanwhile, we integrate a visibility-based viewpoint decision module in MSGNav to resolve the last-mile problem. Extensive experiments on GOAT-Bench and HM3D-OVON datasets demonstrate consistent and notable gains over existing methods, highlighting the effectiveness of the proposed multi-modal scene representations in embodied navigation.

Limitations and future work. Despite these advantages of MSGNav, scene graph-based methods still face low inference efficiency due to the latency of VFMs and VLMs, suggesting future work on faster graph construction and inference for real-time deployment. Additionally, while the "last-mile" problem has been mitigated by the VVD module, it is not fully resolved. Exploring reinforcement learning approaches, e.g. active target recognition, to further solve this challenge is also a way worthy of attention.

References

- [1] Jinze Bai, Shuai Bai, Yunfei Chu, Zeyu Cui, Kai Dang, Xiaodong Deng, Yang Fan, Wenbin Ge, Yu Han, Fei Huang, et al. Owen technical report. *ARXIV*, 2023. 2
- [2] Angel Chang, Angela Dai, Thomas Funkhouser, Maciej Halber, Matthias Niessner, Manolis Savva, Shuran Song, Andy Zeng, and Yinda Zhang. Matterport3d: Learning from rgb-d data in indoor environments. ARXIV, 2017.
- [3] Haonan Chang, Kowndinya Boyalakuntla, Shiyang Lu, Si-wei Cai, Eric Jing, Shreesh Keskar, Shijie Geng, Adeeb Ab-bas, Lifeng Zhou, Kostas Bekris, et al. Context-aware entity grounding with open-vocabulary 3d scene graphs. ARXIV, 2023. 3
- [4] Boyuan Chen, Fei Xia, Brian Ichter, Kanishka Rao, Keerthana Gopalakrishnan, Michael S Ryoo, Austin Stone, and Daniel Kappler. Open-vocabulary queryable scene representations for real world planning. ARXIV, 2022. 3
- [5] Jiaqi Chen, Bingqian Lin, Ran Xu, Zhenhua Chai, Xiaodan Liang, and Kwan-Yee K Wong. Mapgpt: Mapguided prompting with adaptive path planning for visionand-language navigation. *ARXIV*, 2024. 3
- [6] Tianheng Cheng, Lin Song, Yixiao Ge, Wenyu Liu, Xinggang Wang, and Ying Shan. Yolo-world: Real-time open-vocabulary object detection. In CVPR, pages 16901–16911, 2024. 4, 5
- [7] Angela Dai, Angel X Chang, Manolis Savva, Maciej Halber, Thomas Funkhouser, and Matthias Nießner. Scannet: Richly-annotated 3d reconstructions of indoor scenes. In *Proceedings of the IEEE conference on computer vision and pattern recognition*, pages 5828–5839, 2017. 5
- [8] Yilun Du, Chuang Gan, and Phillip Isola. Curious representation learning for embodied intelligence. In *ICCV*, pages 10408–10417, 2021.
- [9] Samir Yitzhak Gadre, Mitchell Wortsman, Gabriel Ilharco, Ludwig Schmidt, and Shuran Song. Cows on pasture: Baselines and benchmarks for language-driven zero-shot object navigation. In CVPR, pages 23171–23181, 2023. 3
- [10] Dylan Goetting, Himanshu Gaurav Singh, and Antonio Loquercio. End-to-end navigation with vision language models: Transforming spatial reasoning into question-answering. ARXIV, 2024. 6, 7
- [11] Qiao Gu, Ali Kuwajerwala, Sacha Morin, Krishna Murthy Jatavallabhula, Bipasha Sen, Aditya Agarwal, Corban Rivera, William Paul, Kirsty Ellis, Rama Chellappa, et al. Conceptgraphs: Open-vocabulary 3d scene graphs for perception and planning. In *ICRA*, pages 5021–5028. IEEE, 2024. 3, 4, 7, 8
- [12] Haodong Hong, Yanyuan Qiao, Sen Wang, Jiajun Liu, and Qi Wu. General scene adaptation for vision-and-language navigation. ARXIV, 2025. 3
- [13] Yue Hu, Junzhe Wu, Ruihan Xu, Hang Liu, Avery Xi, Henry X Liu, Ram Vasudevan, and Maani Ghaffari. Imaginative world modeling with scene graphs for embodied agent navigation. *ARXIV*, 2025. 3
- [14] Aaron Hurst, Adam Lerer, Adam P Goucher, Adam Perelman, Aditya Ramesh, Aidan Clark, AJ Ostrow, Akila Weli-

- hinda, Alan Hayes, Alec Radford, et al. Gpt-4o system card. ARXIV, 2024. 2
- [15] Zihe Ji, Huangxuan Lin, and Yue Gao. Dynavlm: Zero-shot vision-language navigation system with dynamic viewpoints and self-refining graph memory. ARXIV, 2025. 2, 6, 7
- [16] Mukul Khanna, Ram Ramrakhya, Gunjan Chhablani, Sriram Yenamandra, Theophile Gervet, Matthew Chang, Zsolt Kira, Devendra Singh Chaplot, Dhruv Batra, and Roozbeh Mottaghi. Goat-bench: A benchmark for multi-modal lifelong navigation. In CVPR, pages 16373–16383, 2024. 3, 6, 7
- [17] Ue-Hwan Kim, Jin-Man Park, Taek-Jin Song, and Jong-Hwan Kim. 3-d scene graph: A sparse and semantic representation of physical environments for intelligent agents. *TCYB*, 50(12):4921–4933, 2019. 3
- [18] Alexander Kirillov, Eric Mintun, Nikhila Ravi, Hanzi Mao, Chloe Rolland, Laura Gustafson, Tete Xiao, Spencer Whitehead, Alexander C Berg, Wan-Yen Lo, et al. Segment anything. In *ICCV*, pages 4015–4026, 2023. 4
- [19] Jacob Krantz, Theophile Gervet, Karmesh Yadav, Austin Wang, Chris Paxton, Roozbeh Mottaghi, Dhruv Batra, Jitendra Malik, Stefan Lee, and Devendra Singh Chaplot. Navigating to objects specified by images. In *ICCV*, pages 10916–10925, 2023. 3
- [20] Obin Kwon, Jeongho Park, and Songhwai Oh. Renderable neural radiance map for visual navigation. In CVPR, pages 9099–9108, 2023. 3
- [21] Dingbang Li, Wenzhou Chen, and Xin Lin. Tina: Think, interaction, and action framework for zero-shot vision language navigation. In *ICME*, pages 1–6. IEEE, 2024. 3
- [22] Junjie Li, Nan Zhang, Xiaoyang Qu, Kai Lu, Guokuan Li, Jiguang Wan, and Jianzong Wang. Rate-nav: Regionaware termination enhancement for zero-shot object navigation with vision-language models. ARXIV, 2025. 3
- [23] Shilong Liu, Zhaoyang Zeng, Tianhe Ren, Feng Li, Hao Zhang, Jie Yang, Qing Jiang, Chunyuan Li, Jianwei Yang, Hang Su, et al. Grounding dino: Marrying dino with grounded pre-training for open-set object detection. In ECCV, pages 38–55. Springer, 2024. 5
- [24] Yuxing Long, Wenzhe Cai, Hongcheng Wang, Guanqi Zhan, and Hao Dong. Instructnav: Zero-shot system for generic instruction navigation in unexplored environment. ARXIV, 2024. 3
- [25] Yuxing Long, Xiaoqi Li, Wenzhe Cai, and Hao Dong. Discuss before moving: Visual language navigation via multi-expert discussions. In *ICRA*, pages 17380–17387. IEEE, 2024. 3
- [26] Jian Luo, Jian Zhang, Jie Yang, Siwei Huang, and Bo Cai. Learning bird's eye view scene graph and knowledgeinspired policy for embodied visual navigation. KBS, page 113959, 2025. 3
- [27] Matthias Minderer, Alexey Gritsenko, and Neil Houlsby. Scaling open-vocabulary object detection. *NeurIPS*, 36: 72983–73007, 2023. 2, 3
- [28] Alec Radford, Jong Wook Kim, Chris Hallacy, Aditya Ramesh, Gabriel Goh, Sandhini Agarwal, Girish Sastry, Amanda Askell, Pamela Mishkin, Jack Clark, et al. Learning transferable visual models from natural language supervision. In *ICML*, pages 8748–8763. PmLR, 2021. 4

- [29] Alec Radford, Jong Wook Kim, Chris Hallacy, Aditya Ramesh, Gabriel Goh, Sandhini Agarwal, Girish Sastry, Amanda Askell, Pamela Mishkin, Jack Clark, et al. Learning transferable visual models from natural language supervision. In *ICML*, pages 8748–8763. PMLR, 2021. 3
- [30] Abhinav Rajvanshi, Karan Sikka, Xiao Lin, Bhoram Lee, Han-Pang Chiu, and Alvaro Velasquez. Saynav: Grounding large language models for dynamic planning to navigation in new environments. In *ICAPS*, pages 464–474, 2024. 2
- [31] Santhosh K Ramakrishnan, Aaron Gokaslan, Erik Wijmans, Oleksandr Maksymets, Alex Clegg, John Turner, Eric Undersander, Wojciech Galuba, Andrew Westbury, Angel X Chang, et al. Habitat-matterport 3d dataset (hm3d): 1000 large-scale 3d environments for embodied ai. ARXIV, 2021. 2, 5
- [32] Santhosh Kumar Ramakrishnan, Devendra Singh Chaplot, Ziad Al-Halah, Jitendra Malik, and Kristen Grauman. Poni: Potential functions for objectgoal navigation with interaction-free learning. In CVPR, pages 18890–18900, 2022. 3
- [33] Ram Ramrakhya, Dhruv Batra, Erik Wijmans, and Abhishek Das. Pirlnav: Pretraining with imitation and rl finetuning for objectnav. In CVPR, pages 17896–17906, 2023. 7
- [34] Ram Ramrakhya, Dhruv Batra, Erik Wijmans, and Abhishek Das. Pirlnav: Pretraining with imitation and rl finetuning for objectnav. In *CVPR*, pages 17896–17906, 2023. 7
- [35] Ram Ramrakhya, Dhruv Batra, Erik Wijmans, and Abhishek Das. Pirlnav: Pretraining with imitation and rl finetuning for objectnav. In *CVPR*, pages 17896–17906, 2023. 2, 3
- [36] Krishan Rana, Jesse Haviland, Sourav Garg, Jad Abou-Chakra, Ian Reid, and Niko Suenderhauf. Sayplan: Grounding large language models using 3d scene graphs for scalable robot task planning. ARXIV, 2023. 3
- [37] Antoni Rosinol, Arjun Gupta, Marcus Abate, Jingnan Shi, and Luca Carlone. 3d dynamic scene graphs: Actionable spatial perception with places, objects, and humans. ARXIV, 2020. 3
- [38] Tixiao Shan, Abhinav Rajvanshi, Niluthpol Mithun, and Han-Pang Chiu. Graph2nav: 3d object-relation graph generation to robot navigation. *ARXIV*, 2025. 2
- [39] Abdelrhman Werby, Chenguang Huang, Martin Büchner, Abhinav Valada, and Wolfram Burgard. Hierarchical openvocabulary 3d scene graphs for language-grounded robot navigation. In *ICRA*, 2024. 2
- [40] Erik Wijmans, Abhishek Kadian, Ari Morcos, Stefan Lee, Irfan Essa, Devi Parikh, Manolis Savva, and Dhruv Batra. Dd-ppo: Learning near-perfect pointgoal navigators from 2.5 billion frames. ARXIV, 2019. 7
- [41] Erik Wijmans, Abhishek Kadian, Ari Morcos, Stefan Lee, Irfan Essa, Devi Parikh, Manolis Savva, and Dhruv Batra. Dd-ppo: Learning near-perfect pointgoal navigators from 2.5 billion frames. ARXIV, 2019. 3
- [42] Zichen Yan, Rui Huang, Lei He, Shao Guo, and Lin Zhao. Sign: Safety-aware image-goal navigation for autonomous drones via reinforcement learning. ARXIV, 2025. 3
- [43] Yuncong Yang, Han Yang, Jiachen Zhou, Peihao Chen, Hongxin Zhang, Yilun Du, and Chuang Gan. 3d-mem: 3d

- scene memory for embodied exploration and reasoning. In *CVPR*, pages 17294–17303, 2025. 2, 4, 5, 6, 7, 8
- [44] Hang Yin, Xiuwei Xu, Zhenyu Wu, Jie Zhou, and Jiwen Lu. Sg-nav: Online 3d scene graph prompting for llm-based zero-shot object navigation. *NeurIPS*, 37:5285–5307, 2024. 2, 3, 4, 6
- [45] Hang Yin, Xiuwei Xu, Linqing Zhao, Ziwei Wang, Jie Zhou, and Jiwen Lu. Unigoal: Towards universal zero-shot goaloriented navigation. In CVPR, pages 19057–19066, 2025. 2, 3, 4
- [46] Naoki Yokoyama, Sehoon Ha, Dhruv Batra, Jiuguang Wang, and Bernadette Bucher. vlfm: Vision-language frontier maps for zero-shot semantic navigation. In *ICRA*, pages 42–48. IEEE, 2024. 3, 7
- [47] Naoki Yokoyama, Ram Ramrakhya, Abhishek Das, Dhruv Batra, and Sehoon Ha. Hm3d-ovon: A dataset and benchmark for open-vocabulary object goal navigation. In *IROS*, pages 5543–5550. IEEE, 2024. 2, 3, 6, 7
- [48] Bangguo Yu, Yuzhen Liu, Lei Han, Hamidreza Kasaei, Tingguang Li, and Ming Cao. Vln-game: Visionlanguage equilibrium search for zero-shot semantic navigation. ARXIV, 2024. 2
- [49] Zhaohuan Zhan, Lisha Yu, Sijie Yu, and Guang Tan. Mc-gpt: Empowering vision-and-language navigation with memory map and reasoning chains. ARXIV, 2024. 3
- [50] Jiazhao Zhang, Kunyu Wang, Shaoan Wang, Minghan Li, Haoran Liu, Songlin Wei, Zhongyuan Wang, Zhizheng Zhang, and He Wang. Uni-navid: A video-based visionlanguage-action model for unifying embodied navigation tasks. ARXIV, 2024. 7
- [51] Yue Zhang, Ziqiao Ma, Jialu Li, Yanyuan Qiao, Zun Wang, Joyce Chai, Qi Wu, Mohit Bansal, and Parisa Kordjamshidi. Vision-and-language navigation today and tomorrow: A survey in the era of foundation models. ARXIV, 2024. 2
- [52] Gengze Zhou, Yicong Hong, and Qi Wu. Navgpt: Explicit reasoning in vision-and-language navigation with large language models. In *AAAI*, pages 7641–7649, 2024. 3
- [53] Kaiwen Zhou, Kaizhi Zheng, Connor Pryor, Yilin Shen, Hongxia Jin, Lise Getoor, and Xin Eric Wang. Esc: Exploration with soft commonsense constraints for zero-shot object navigation. In *ICML*, pages 42829–42842. PMLR, 2023. 3
- [54] Ziyu Zhu, Xilin Wang, Yixuan Li, Zhuofan Zhang, Xiaojian Ma, Yixin Chen, Baoxiong Jia, Wei Liang, Qian Yu, Zhidong Deng, et al. Move to understand a 3d scene: Bridging visual grounding and exploration for efficient and versatile embodied navigation. ARXIV, 2025. 2, 7
- [55] Filippo Ziliotto, Tommaso Campari, Luciano Serafini, and Lamberto Ballan. Tango: training-free embodied ai agents for open-world tasks. In CVPR, pages 24603–24613, 2025. 2, 7